ЖЭТФ, 2007, том 132, вып. 5 (11), стр. 1052–1063 

# ON THE PRODUCTION OF FLAT ELECTRON BUNCHES FOR LASER WAKEFIELD ACCELERATION

***M. Kando, Y. Fukuda, H. Kotaki, J. Koga, S. V. Bulanov*, T. Tajima***

*Kansai Photon Science Institute, Japan Atomic Energy Agency*
*619-0215, Kyoto, Japan*

***A. Chao, R. Pitthan***

*Stanford Linear Accelerator Center*
*94025, California, USA*

***K.-P. Schuler***

*DESY, Deutsches Elektronen-Synchrotron*
*22603, Hamburg, Germany*

***A. G. Zhidkov**, K. Nemoto***

*Central Research Institute of Electric Power Industry*
*240-0196, Kanagawa, Japan*

Received April 3, 2007

We suggest a novel method for injection of electrons into the acceleration phase of particle accelerators, producing low-emittance beams appropriate even for the demanding high-energy linear collider specifications. We discuss the injection mechanism into the acceleration phase of the wakefield in a plasma behind a high-intensity laser pulse, which takes advantage of the laser polarization and focusing. The scheme uses the structurally stable regime of transverse wakewave breaking, when electron trajectory self-intersection leads to the formation of a flat electron bunch. As shown in three-dimensional particle-in-cell simulations of the interaction of a laser pulse elongated in a transverse direction with an underdense plasma, the electrons injected via the transverse wakewave breaking and accelerated by the wakewave perform betatron oscillations with different amplitudes and frequencies along the two transverse coordinates. The polarization and focusing geometry lead to a way to produce relativistic electron bunches with asymmetric emittance (flat beam). An approach for generating flat laser-accelerated ion beams is briefly discussed.

PACS: 52.38.Kd, 41.75.Jv, 52.38.Hb, 52.38.-r

## 1. INTRODUCTION

Electron accelerators with energies of many GeV and low emittance are needed for coherent light sources and linear colliders. The laser acceleration of charged particles provides a promising approach toward such development in a compact way, avoiding some of the complications arising due to additional requirements of asymmetric emittance for linear colliders, as outlined below. In the laser wake-field accelerator (LWFA) concept, electrons are accelerated by the longitudinal electric field created in an underdense plasma by a short high-intensity laser pulse [1]. Electrons injected by conventional accelerators, self-injected by nonlinear wakewave breaking (for details, see papers [2–4] and review articles [5] and the references therein), or injected in a multiple laser pulse configuration [6] can achieve energies substantially higher than the initial injection energies. Although the understanding and production of high-intensity ($\approx$ nC) and low-emittance ($\approx$ 2–3 mm $\cdot$ mrad) electron beams via laser plasma interaction has made rapid progress [5, 7–12], applica-

*Also at Prokhorov Institute of General Physics, Russian Academy of Sciences, 119991, Moscow, Russia.
**E-mail: zhidkov@criepi.denken.or.jp

tions to coherent light sources and linear colliders still demand further advances. A symmetric emittance of about 1 mm · mrad is needed for coherent light sources to reach X-ray wavelengths of the order of 1 Å [13]. Linear electron–positron colliders need asymmetric emittances and polarized electrons, with the smaller vertical emittance required to be of the order of 0.1 mm · mrad. The asymmetric emittances (flat beam[1)]) are needed to reduce the beam-induced synchrotron radiation (beamstrahlung) in the interaction (see below), and electron polarization is required because the effective luminosity can be up to 2 orders of magnitude larger (depending on the process), as shown by the SLD experiment at the Stanford Linear Collider (SLC) [14]. Additionally, positron beam polarization is desirable because certain processes can be measured with a higher signal-to-noise ratio due to the additional positron polarization, and it allows measuring transverse cross sections [15]. The capability to selectively suppress unwanted background processes is especially desired in the search for new physics.

In producing 1 GeV range laser-accelerated electron bunches [12], a more quantitative evaluation of the differing requirements of major applications using GeV electrons is needed. These requirements include, in the order of increasing beam quality, 1) fixed target–electron beam interactions, 2) synchrotron and coherent light sources and 3) colliding electron (positron) beam configurations.

1) For fixed-target applications, the electron beam emittance is less important because the luminosity is determined by the beam charge and the target thickness [16]. In this application, the electron polarization can play a role and enhance the effective luminosity.

2) In the case of the GeV electron beam use for coherent light sources, e.g., for linac light sources, low emittance is important, because radiation from a high-emittance beam fails to be coherent. This application requires small emittances, of the order of 1 mm · mrad for 1 Å wavelength, but a small spot size is not necessary.

3) For colliding electron beams, the emittance determines the minimum achievable spot size and is therefore directly related to the maximum luminosity. Depending on the electron energy, the required spot size is approximately equal to 400 nm for 100 GeV electrons, and 5 nm (small dimension) for 1 TeV colliders [17]. Required for colliders in addition are the electron beam polarization (80 % or more) and flat beams with the beam size aspect ratio about 100, in order to reduce beamstrahlung losses and electron–positron pair production [14, 18].

The conditions to have beams of high electric charge and low emittance are contradictory, because space charge effects make the transverse emittance grow [19].

As is known, the emittance is calculated as the spot size $\sigma_x$ times the divergence $\sigma'_x$, both determined at a beam waist (or a pin hole); that is, the transverse emittance is $\varepsilon = \sigma_x \sigma'_x$. In addition, the normalized emittance, defined as $\varepsilon_N = \gamma_e \varepsilon$, is an adiabatic invariant under beam acceleration, where $\gamma_e$ is the electron relativistic gamma factor. The values of emittance quoted above refer to the normalized emittances.

If we consider LWFA-produced electrons, we see femtosecond-range electron bunches accelerated to hundreds of MeV, and driven out of the plasma. The energy spectrum has a quasi-mono-energetic form [8–12, 20], mainly because fast electrons reach the maximum energy and are localized at the top of the separatrix in the $x$, $p_x$ phase plane [21, 22]. We remark concerning two properties of LWFA ejected relativistic electrons: a) the bunch length times the energy spread, the longitudinal emittance, is comparable to that of conventional radiofrequency sources (in the range of MeV·ps), while the very short bunch length is achieved even without bunch compression, and b) the micron-size transverse spot of the initial electron bunch corresponds to the laser spot size, which may in turn lead to a small transverse emittance. At present, the emittance requirements, including the asymmetry, are satisfied with the use of expensive damping rings, which often yield long bunches and therefore require subsequent bunch compressions. There is another research and development effort underway to produce asymmetric beams using radiofrequency guns [23].

In the present paper, we consider the regime when the electron injection into the acceleration phase of a wakefield occurs due to nonlinear wave-breaking of a Langmuir wave, as in Refs. [8–11]. As is well known, there are several other injection mechanisms, e.g., the optical injection proposed in Ref. [6] and experimentally realized in Ref. [24]. Discussing the optical injection is beyond the scope of this paper. The breaking of the Langmuir wave, known since Refs. [25, 26], has been studied theoretically and experimentally (see Ref. [5] and the references therein). It is important to note that the realization of resilience against wave-

[1)] This paper addresses both laser-plasma and accelerator physics issues. One frequent confusion in the nomenclature is the use of the term "flat beam". In accelerator physics, flat beam means an asymmetric spot size (created with an asymmetric emittance). In laser physics, a flat beam is one with a large focal length, and the means to achieve an asymmetric spot size is a "line focus".

breaking in the relativistic regime in the longitudinal direction led to the original LWFA suggestion [1]. In the non-one-dimensional case and in the case of an inhomogeneous plasma density, the wake wave-breaking acquires features that allow manipulation of the injected electron bunch parameters. For example, properties of the transverse wake wave-breaking [27] were used in Refs. [8, 20, 28] in order to explain nonlinear wake evolution and electron acceleration in homogeneous and inhomogeneous plasmas. In addition, longitudinal breaking was invoked to describe electron self-injection in homogeneous plasmas [29, 30], and the controllable electron injection regimes in plasmas with a tailored density profile [31].

In what follows, we formulate an approach for producing asymmetric emittance electron bunches by using asymmetric laser pulse focusing for the laser wakefield acceleration, when the transverse wake wave breaking leads to the formation of an electron bunch elongated along the transverse direction.

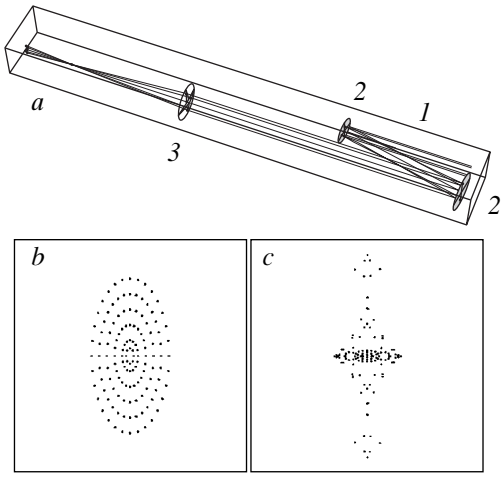


**Fig. 1.** An example of the optical system to achieve an asymmetric focal spot from a symmetric laser beam: *a*) optical layout: *1* — symmetric laser beam, *2* — cylindrical relecting mirrors, *3* — test focusing lens; *b*) near-field pattern on the test lens with the transverse size $50 \times 100$ mm$^2$; *c*) far-field pattern in the focus region with the size $125 \times 500$ $\mu$m$^2$

## 2. LASER LINE FOCUS

In laser systems based on chirped pulse amplification (CPA), laser pulses have a Gaussian (TEM00)-like spatial profile. There are several schemes to achieve a line focus with an asymmetric transverse spatial profile. An astigmatism on the sagittal plane of a spherical mirror is used. This technique was applied to produce transient X-ray lasers. This scheme can generate a large aspect ratio of 300:1, but the focusing depth is limited and a time difference for arriving at the focus arises [32]. A slightly misaligned off-axis parabolic mirror generates astigmatism, resulting in an asymmetric focal spot. A toroidal mirror can also be used. Here, we propose to use a pair of reflective cylindrical mirrors. Cylindrical mirrors are easy to fabricate and are cost-saving. A large value of the astigmatism of cylindrical mirrors placed off-axis can be improved when the incident angle is chosen properly. Figure 1 shows an example of the asymmetric laser focal spot in the configuration with a pair of cylindrical mirrors. In this particular case, the focal lengths in the perpendicular planes are equal to $f_1 = -500$ mm and $f_2 = 1000$ mm. In this configuration, a round laser beam is transformed into a 1:2 (horizontal and vertical sizes) asymmetric transverse profile as seen in Fig. 1*b*. To plot the asymmetric beam profile shown in Fig. 1*c*, a plane-convex lens optical system was considered. In the actual experiment, an off-axis parabolic mirror can be used instead of the lens. We note that further studies are needed to examine the effect of effective pulse elongation, which occurs if these line focus techniques are used, for the wakefield generation.

## 3. STRUCTURE OF TRANSVERSE WAKE WAVE BREAKING

Due to a nonlinear dependence of the Langmuir wave frequency on its amplitude, constant-phase surfaces in the wake wave give rise to a paraboloidal form [33, 34]. The curvature of constant-phase surfaces increases with the distance from the laser pulse until the curvature radius $R$ becomes comparable to the electron displacement $\zeta$ in the wake, leading to electron trajectory self-intersection. This is the so-called regime of transverse wake breaking, which may result in the electron injection into the acceleration phase [27]. Along the lines of Ref. [27], we consider a wakefield plasma wave excited by a laser pulse of finite width. The condition of the wake excitation determines the wake frequency and wavenumber $\omega_w$ and $k_w$. Here, $\omega_w = k_w v_g$ and $v_g$ is the group velocity of the driver laser pulse. The wake wave frequency, equal to the local value of the Langmuir frequency, depends on the transverse coordinates $y$ and $z$. This dependence arises due to the plasma outward motion caused by the laser pulse ponderomotive pressure and by the relativistic dependence

of the Langmuir frequency on the wave amplitude. The dependence on the wave amplitude is determined by the laser pulse transverse shape, which can be approximated in the vicinity of the axis as

$$a(y,z) \approx a_0 \left[1 - (y/s_y)^2 - (z/s_z)^2\right].$$

It therefore has an elliptic form in the transverse plane. The wake frequency near the axis may be approximated by the simple expression

$$\omega_w(y,z) \approx \omega_{w,0} + \Delta\omega_w \left[\left(\frac{y}{s_y}\right)^2 + \left(\frac{z}{s_z}\right)^2\right],$$

where $s_y$ and $s_z$ are related to the curvature radii in the $y$ and $z$ directions, and $\Delta\omega_w$ is the difference between the Langmuir frequency outside and on the axis of the wake field, $\omega_{w,0}$. From the expression for constant-phase surfaces in the wake wave,

$$\psi_w(x,y,z,t) = \omega_w(y,z)\left(t - \frac{x}{v_g}\right) = \text{const},$$

it follows that their curvature increases with the distance $l$ from the laser pulse front: the curvature radii decrease as $R_y = \omega_{w,0}s_y^2/2\Delta\omega_w l$ and $R_z = \omega_{w,0}s_z^2/2\Delta\omega_w l$ with $l = \psi_w v_g/\omega_{w,0}$.

We write the equation for the constant-phase surface in the form

$$\mathbf{M}_0(y_0,z_0) = \left(\frac{y_0^2}{2R_y} + \frac{z_0^2}{2R_z}\right)\mathbf{e}_x + y_0\mathbf{e}_y + z_0\mathbf{e}_z, \quad (1)$$

where $\mathbf{e}_x$, $\mathbf{e}_y$, and $\mathbf{e}_z$ are the unit vectors along the $x$, $y$, and $z$ axes. In a nonlinear wake, the actual position of the constant-phase surface is given by the equation

$$\mathbf{M}(y_0,z_0) = \mathbf{M}_0(y_0,z_0) + \zeta\mathbf{n}(y_0,z_0), \quad (2)$$

where $\zeta$ is the amplitude of the electron displacement and

$$\mathbf{n}(y_0,z_0) = \frac{\partial_{y_0}\mathbf{M}\times\partial_{z_0}\mathbf{M}}{|\partial_{y_0}\mathbf{M}\times\partial_{z_0}\mathbf{M}|} \quad (3)$$

is the unit vector normal to the constant-phase surface. In the case where the surface is given by Eq. (1), the normal vector is

$$\mathbf{n}(y_0,z_0) = \left[1 + \left(\frac{y_0}{R_y}\right)^2 + \left(\frac{z_0}{R_z}\right)^2\right]^{-1/2} \times \left(\mathbf{e}_x + \frac{y_0}{R_y}\mathbf{e}_y + \frac{z_0}{R_z}\mathbf{e}_z\right). \quad (4)$$

Writing Eq. (2) in components, we obtain

$$x = \frac{y_0^2}{2R_y} + \frac{z_0^2}{2R_z} + \frac{\zeta}{\sqrt{1 + (y_0/R_y)^2 + (z_0/R_z)^2}}, \quad (5)$$

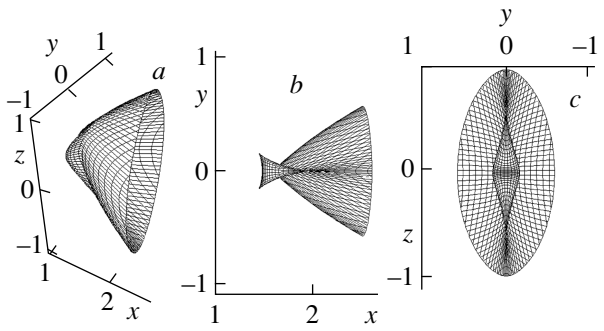


**Fig. 2.** The constant-phase surface for $R_y = 1$, $R_z = 1.666$, and $\zeta = 1.5$, in the $x$, $y$, $z$ space ($a$); and its projections on the $(x,y)$ ($b$); and $(y,z)$ ($c$) planes

$$y = y_0 - \frac{\zeta y_0}{R_y\sqrt{1 + (y_0/R_y)^2 + (z_0/R_z)^2}}, \quad (6)$$

$$z = z_0 - \frac{\zeta z_0}{R_z\sqrt{1 + (y_0/R_y)^2 + (z_0/R_z)^2}}. \quad (7)$$

For a suffuciently large electron displacement $\zeta$, the map given by Eqs. (4)–(7) has a singularity, at which the constant surface folds. The condition for the singularity occurrence corresponds to the $\zeta$ value for which the Jacobian of the transformation from the variables $(y,z)$ to the variables $(y_0,z_0)$ vanishes, $|\partial(y,z)/\partial(y_0,z_0)| = 0$. Assuming the curvature radius in the $z$ direction to be larger than in the $y$ direction, $R_z > R_y$, in the limit of relatively small but finite values of $y_0/R_y$ and $z_0/R_z$, we find that the position of the singularity in the $y_0, z_0$ plane is determined by the equation

$$2R_y = \zeta\left[2 - 3(y_0/R_y)^2 - (z_0/R_z)^2\right]. \quad (8)$$

This equation has a solution if $\zeta \geq R_y$, i.e., the displacement is larger than the curvature radius. For $\zeta > R_y$, the curve determined by Eq. (8) is an ellipse with the semi-axes $R_y\sqrt{2(\zeta - R_y)/3\zeta}$ and $R_z\sqrt{2(\zeta - R_y)/\zeta}$ in the $y_0$ and $z_0$ directions.

We plot the surface in the $x$, $y$, $z$ space in which $\zeta = 0$ is the paraboloid $x = y_0^2/2R_y + z_0^2/2R_z$, $y = y_0$, $z = z_0$. With Eqs. (5)–(7), we obtain the constant-phase surfaces in the cases with $\zeta \neq 0$ presented in Figs. 2 and 3. In both cases, in Figs. 2 and 3, the projections of the constant-phase surface onto the $x, y$ plane have the form of a "swallow tail". This corresponds to one of the forms of fundamental catastrophes (see [35]).

When the displacement value is between the curvature radii, i.e., $R_y < \zeta < R_z$, as in the case shown in

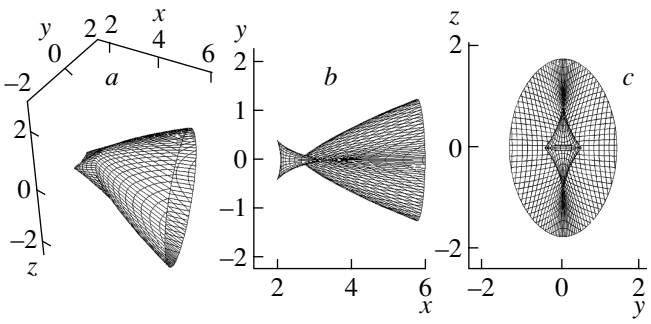


**Fig. 3.** The constant-phase surface for $R_y = 1$, $R_z = 1.666$, and $\zeta = 2$, in the $x$, $y$, $z$ space ($a$); and its projections on the $(x, y)$ ($b$); and $(y, z)$ ($c$) planes

Fig. 2, the singularity in the $(y, z)$ plane is elongated along the $z$ axis. On the other hand, if $R_y < R_z < \zeta$, the singularity in the $(y, z)$ plane is elongated along the $y$ axis, as shown in Fig. 3$c$. These types of singularities are typical, or, in other words, are structurally stable. In 3D configurations, they correspond to the transverse wave breaking with the injection into the acceleration phase of flat electron bunches.

In the axially symmetric geometry, when the curvature radii along the $y$ and $z$ directions are equal to each other, $R_y = R_z$, the injected electron bunch also has an axial symmetry. However, this configuration is not structurally stable and small perturbations of a general type transform it into a structurally stable configuration with an axially nonsymmetric electron bunch. We point out that in the case of a gradual increase in the wake wave curvature, the first breaking occurs when the electron displacement becomes greater than the minimal curvature radius, e.g., when $R_y < \zeta < R_z$, and the injected electron bunch is elongated along the minimal curvature direction as in Fig. 2.

After the electron trajectory self-intersection has occurred, the injected electrons are accelerated and perform betatron oscillations in the transverse direction. This stage of the electron bunch evolution is discussed in Secs. 4 and 5 below, where we present the results of the particle-in-cell (PIC) simulations and the analytic theory of betatron oscillations when the effects of the space charge are taken into account.

## 4. RESULTS OF SIMULATIONS OF TRANSVERSE WAKE WAVE BREAKING AND ELECTRON BUNCH INJECTION

The paraboloidal structures of the wake plasma wave have been seen routinely in the three-dimensional particle-in-cell simulations of high-intensity laser pulse propagation in underdense plasmas (e.g., see Refs. [36, 37], where the laser pulse frequency upshifting was discussed in counter- and co-propagating two-pulse-interaction configurations). The paraboloidal wake plasma waves were observed in experiments involving laser pulse interactions with an underdense plasma [34]. In Refs. [10, 37], 3D PIC simulations distinctly show the "swallow tail" structure in the electron density distribution formed in the nonlinear wake wave. In this section, we present 3D PIC simulation results for the electron bunch injection, which clearly demonstrate the elongated electron bunch generation during the transverse wake wave breaking. We use the electromagnetic relativistic PIC computer code FPLaser3D [30], which exploits the moving window technique and the density decomposition scheme of the current assignment with bell-shaped quasiparticles [38]; this current-weighting scheme significantly reduces the unphysical numerical effects of the standard PIC method.

The flat electron bunch injection is seen in Fig. 4, where the results of the simulations of the ultrashort laser-pulse interaction with an underdense plasma target are shown. A linearly polarized laser pulse with the electric field along the $z$ direction and with the wavelength $\lambda = 0.8$ $\mu$m has the irradiance $I = 10^{20}$ W/cm$^2$. The pulse duration is 27 fs, and the pulse is focused into a spot with the diameter 16 $\mu$m. The laser pulse propagates along the $x$ direction from the right to the left in a plasma with the density $n_e = 10^{19}$ cm$^{-3}$. The simulations were performed with the use of "the moving window" technique in a simulation box of size $80 \times 56 \times 56\lambda^3$. The mesh sizes in the direction of the laser pulse propagation and in the transverse direction are $\Delta x = \lambda/20$ and $\Delta y = \Delta z = \lambda/10$, with 8 particles (electrons and protons) per cell. In Fig. 4, where the electron density distribution in the $z = 0$ plane ($a$), in the $y = 0$ plane ($b$), and in the $x + ct = 315\lambda$ plane ($c$) are presented, we distinctly see fast electron bunches injected into the second period of the wake wave. The electron bunch width in the $z$-direction is approximately two times larger than in the $y$-direction. The flat electron bunch formation is also seen in Fig. 5, where the density distributions of fast electrons (with $p_x > 200$ MeV/$c$) in the $z = 0$ plane ($a$) and in the $y = 0$ plane ($b$) are presented. We note that electron oscillations in the perpendicular directions, along the $y$ and $z$ axes, have different frequencies, as is distinctly seen in Fig. 5. The electron energy spectrum presented in Fig. 6 demonstrates a quasi-mono-energetic component at the energy around 100 MeV with the maximal

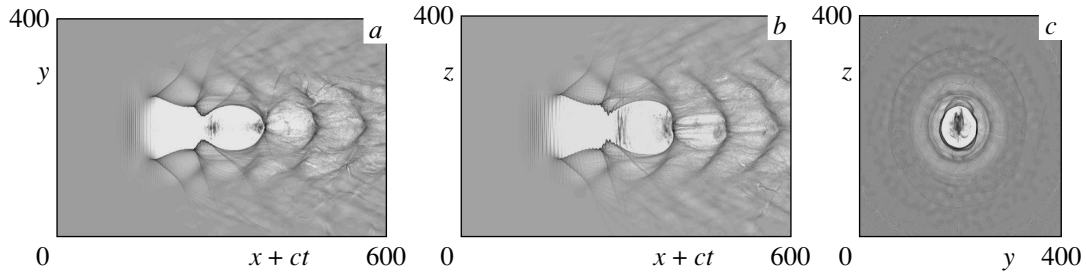


**Fig. 4.** Results of the 3D PIC simulations: the electron density distribution in the $z = 0$ plane ($a$); in the $y = 0$ plane ($b$); and in the $x + ct = 315\lambda$ plane ($c$). The laser pulse propagates from left to right in the $x$ direction

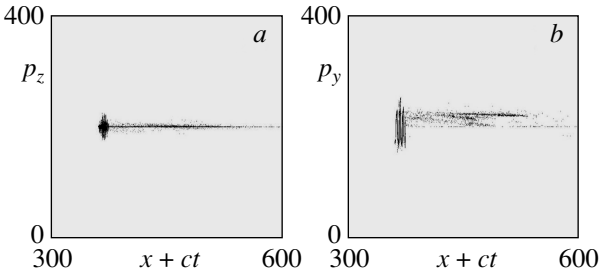


**Fig. 5.** Fast electron (with $p_x > 200$ MeV/$c$) density distribution in the $z = 0$ plane ($a$); and in the $y = 0$ plane ($b$)

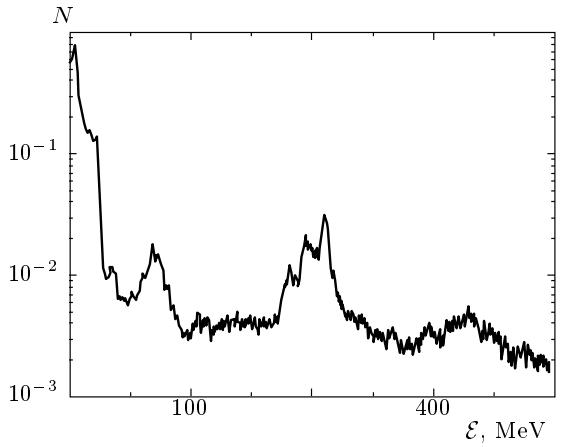


**Fig. 6.** Electron energy spectrum

energy equal to 200 MeV. The geometrical emittance for the electrons with the energy $E > 100$ MeV is estimated as $10^{-4}\pi$ mm · mrad.

In the case under consideration, the transverse asymmetry of the wake breaking and the electron bunch generation occurs due to the effect of the linear polarization of the laser. As found in Ref. [39], the linearly polarized laser pulse generates axially asymmetric self-focusing channels and a wake with different amplitudes in the directions along and perpendicular to the polarization direction. We note that the wakefield accelerated electron bunches with an elliptic form in the transverse direction have been observed in the experiments in Ref. [40], where the transverse elongation was attributed to the effects of the linear polarization of the laser pulse driver.

## 5. EQUILIBRIUM AND BETATRON OSCILLATIONS OF A TRANSVERSALLY ELONGATED ELECTRON BUNCH WITH SPACE CHARGE

In this section, we consider the electron bunch equilibrium configuration inside the wake when its transverse size is substantially smaller than its length. We describe betatron oscillations of the bunch in the transverse direction. We assume that the longitudinal (along the $x$ axis) scale length of the fast electron bunch is much greater than its scale length in the transverse direction. Below, we therefore assume that the wakefield and the electron bunch are homogeneous along the $x$ axis. Such an approximation may be valid in the near-axis region of the wake when the injection time is of the order of the electron acceleration time.

Betatron oscillations of electrons moving inside the wake wave occur due to the transverse component of the wake electric field vanishing along the axis and having a linear dependence on the transverse coordinates $y$ and $z$ in the vicinity of the axis: $\mathbf{E}_\perp = E_y\mathbf{e}_y + E_z\mathbf{e}_z$ with the components $E_y$ and $E_z$ dependent on the specific form of the wakefield. The effects of the magnetic field, which is self-generated in the regular wake wave, are substantially weaker than the electric field effects (e.g., see Ref. [18]), and we neglect them in our model for simplicity. On the other hand, the pinching by the

magnetic field generated by the electric current carried by fast electrons partially compensates the repelling force due to the electron space charge and we incorporate its effects into our description.

We assume that the transverse cross section of the wake wave has an elliptic form with the semi-axes equal to $R_W A_{22}$ and $R_W A_{33}$, with $R_W$ being the transverse scale length. The positive electric charge density in the wake is $en_0$. Using the Dirichlet formula for the electric field of a uniformly charged elliptic cylinder (see Ref. [41] for the explanations of the Dirichlet formalism for the solution of the Poisson equation in confocal ellipsoidal coordinates), we write the transverse electric field originating from the electric charge separation inside the wake as

$$E_y^{WF}\mathbf{e}_y + E_z^{WF}\mathbf{e}_z = \frac{4\pi e n_0}{A_{22}+A_{33}}(A_{33}y\mathbf{e}_y + A_{22}z\mathbf{e}_z). \quad (9)$$

Within the framework of the test-particle approximation, when we can neglect the effects of the electric and magnetic field produced by the fast electron bunch, the relativistic electron motion in the electric field given by Eq. (9) corresponds to the betatron oscillations. It is easy to obtain that the oscillations are performed along the $y$ and $z$ axes with the respective frequencies

$$\omega_1 = \omega_b\sqrt{\frac{A_{33}}{A_{22}+A_{33}}}, \quad \omega_2 = \omega_b\sqrt{\frac{A_{22}}{A_{22}+A_{33}}}, \quad (10)$$

which do not coincide. Here, $\omega_b = \omega_{pe}/\sqrt{\gamma_e}$ with the electron gamma factor $\gamma_e$ and the Langmuir frequency $\omega_{pe} = \sqrt{4\pi n_0 e^2/m_e}$. The structure of the mode is given by the relations

$$\begin{pmatrix} \delta a_{22} \\ \delta a_{33} \end{pmatrix} = \begin{pmatrix} \sum\limits_{\pm} C_{1,\pm}\exp(\pm i\omega_1 t) \\ \sum\limits_{\pm} C_{2,\pm}\exp(\pm i\omega_2 t) \end{pmatrix}, \quad (11)$$

where $C_{1,\pm}$ and $C_{2,\pm}$ are constants determined by the initial conditions. Here and below, we assume for simplicity that the electron gamma factor $\gamma_e$ is independent of time. The time dependence of $\gamma_e$ can easily be incorporated into our model similarly to Ref. [21], where the betatron oscillations were studied assuming an axial symmetry of the wake and electron bunch.

We now take the space charge effects generating electric and magnetic fields from the electron bunch into account. As was done above, in order to find the electric and magnetic fields $\mathbf{E}_\perp^b$ and $\mathbf{B}_\perp^b$ generated by the elliptic cylindrical electron bunch, we use the Dirichlet formulas. We write expressions for the electric and magnetic fields as

$$E_y^b\mathbf{e}_y + E_z^b\mathbf{e}_z = \frac{4eN_b}{r_b^2(a_{22}+a_{33})}(a_{33}y\mathbf{e}_y + a_{22}z\mathbf{e}_z) \quad (12)$$

and

$$B_y^b\mathbf{e}_y + B_z^b\mathbf{e}_z = \frac{4eN_b v_b}{r_b^2 c(a_{22}+a_{33})}(a_{33}z\mathbf{e}_y - a_{22}y\mathbf{e}_z), \quad (13)$$

where $r_b a_{22}$ and $r_b a_{33}$ are the electron bunch semi-axes in the transverse plane, $v_b$ and $N_b$ are the electron velocity along the $x$ axis and the number of electrons per unit length, and $r_b$ is a typical transverse size of the bunch.

The equations of the motion of a fluid element of the electron bunch in the transverse direction are

$$\partial_t n_b + \nabla_\perp(\mathbf{v}_\perp n_b) = 0, \quad (14)$$

$$\partial_t \mathbf{p}_\perp + (\mathbf{v}_\perp\cdot\nabla_\perp)\mathbf{p}_\perp = e\left(\mathbf{E}_\perp \times \frac{\mathbf{v}_\perp\times\mathbf{B}_\perp}{c}\right), \quad (15)$$

where the electron density $n_b(y,z,t)$ and the transverse component of the electron momentum

$$\mathbf{p}_\perp(y,z,t) = p_y(y,z,t)\mathbf{e}_y + p_z(y,z,t)\mathbf{e}_z$$

depend on the coordinates $y$ and $z$ and time $t$. The operator $\nabla_\perp$ is given by $\nabla_\perp = \partial_y\mathbf{e}_y + \partial_z\mathbf{e}_z$.

For the electric and magnetic fields linearly dependent on the coordinates, as given by Eqs. (9), (12), and (13), the equations of the bunch motion admit a self-similar solution, which describes the fluid motion with a homogeneous deformation [42]. Within the framework of the homogeneous deformation approximation, the relation between the Euler ($x_i$) and Lagrange ($x_i^0$) coordinates has the form

$$x_i = a_{ij}(t)x_j^0, \quad (16)$$

where $a_{ij}$ is a deformation matrix with time-dependent components. Summation over repeated indices is assumed. Differentiating this relation with respect to time, we find that the velocity of the electron fluid element is given by $v_i = w_{ij}(t)x_j$ with $w_{ij} = \dot{a}_{ik}a_{kj}^{-1}$. Here, $a_{kj}^{-1}$ is the inverse matrix to the matrix $a_{ij}$. A kinematical interpretation of the velocity gradient matrix $w_{ij}$ is provided by analyzing the relative motion of two neighboring fluid particles [43]. The particles we consider are separated by $\delta x_i$. The relative velocity $\delta v_i$ can be written as

$$\delta v_i = \partial_j v_i \delta x_j = w_{ij}\delta x_j = \Xi_{ij}\delta x_j + \Omega_{ij}\delta x_j,$$

where $\partial_i = \mathbf{e}_y\partial_y + \mathbf{e}_z\partial_z$; the tensors $\Xi_{ij}$ and $\Omega_{ij}$ are given by

$$\Xi_{ij} = \frac{\partial_j v_i + \partial_i v_j}{2}, \quad \Omega_{ij} = \frac{\partial_j v_i - \partial_i v_j}{2} = -\frac{\varepsilon_{ijk}\omega_k}{2}$$

with $\varepsilon_{ijk}$ being the antisymmetric Ricci tensor. The vector $\omega_k$ is the fluid vorticity $\boldsymbol{\omega} = \nabla\times\mathbf{v}$. The term

$\Xi_{ij}\delta x_j$ describes pure straining motion and $\Omega_{ij}\delta x_j$ describes rigid-body rotation.

In the approximation $|\mathbf{p}_\perp| \ll p_x$, the transverse component of the momentum can be written as $\mathbf{p}_\perp = m_e\gamma_e(v_y\mathbf{e}_y + v_z\mathbf{e}_z)$ with the gamma factor $\gamma_e = (1 - v_b^2/c^2)^{-1/2}$ calculated for the longitudinal energy of fast electrons. In this case, we obtain

$$p_{t,i} = m_e\gamma_e w_{ij}x_j \equiv m_e\gamma_e\dot{a}_{ij}x_j^0.$$

In what follows, we consider the case of curl-free motion, $\nabla_\perp \times \mathbf{p}_\perp = 0$, i.e., the vanishing matrix $\Omega_{ij}$. This corresponds to the diagonal form of the deformation matrix: $a_{ij} = \mathrm{diag}\{1, a_{22}, a_{33}\}$. Assuming the electron density to be homogeneous and substituting the expression $v_i = w_{ij}(t)x_j$ with $w_{ij} = \dot{a}_{ik}a_{kj}^{-1}$ for the electron velocity in continuity equation (13), we find that the electron density inside the bunch is given by

$$n_b(t) = n_b(0)\left(\frac{\det a_{ij}(0)}{\det a_{ij}(t)}\right). \qquad (17)$$

In the case under consideration, $\det a_{ij} = a_{22}a_{33}$.

To illustrate the property of the motion with homogeneous deformation, we consider the simplest example of the dynamics of a pressureless gas for which the deformation matrix satisfies the equation $\ddot{a}_{ij} = 0$ with the initial conditions $a_{ij} = \delta_{ij}$ and $\dot{a}_{ij}(0) = w_{ij}(0)$. The solution of this equation is $a_{ij}(t) = \delta_{ij} + w_{ij}(0)t$. The catastrophe corresponds to the situation where the determinant of $a_{ij}$ vanishes, $\det a_{ij}(t_s) = 0$, and the beam density tends to infinity in accordance with Eq. (17), $n_b(t_s) = \infty$. If the initial matrix of the fluid velocity gradients is diagonal,

$$w_{ij}(0) = \mathrm{diag}\{0, w_{22}(0), w_{33}(0)\},$$

the deformation matrix is equal to

$$a_{ij}(t) = \mathrm{diag}\{1, 1 + w_{22}(0)t, 1 + w_{33}(0)t\},$$

with

$$\det a_{ij}(t) = (1 + w_{22}(0)t)\,(1 + w_{33}(0)t)\,.$$

A singularity occurs when either $t_s = -1/w_{22}(0)$ or $t_s = -1/w_{33}(0)$. The singularity occurs as a line in 3D space for $w_{22}(0)$ and $w_{33}(0)$ being equal and both negative, and the singularity appears as a surface in 3D space when just one value among $w_{22}(0)$ and $w_{33}(0)$ is negative. The generic case corresponds to the situation where just one value among $w_{22}(0)$ and $w_{33}(0)$ is negative. This means that in the generic case, the singularity develops as a surface. We note that such a type of singularity on a surface has been studied in detail in applications of nonlinear dynamics of the gravitational instability [44] and in the theory of magnetic field line reconnection in high-conductivity plasmas [45].

Because the number of electrons per unit length of the elliptical cylinder with the semi-axes $a = r_b a_{22}$ and $b = r_b a_{33}$ is equal to $N_b = n_b\pi r_b^2 a_{22}a_{33}$, we can rewrite Eq. (17) as $n_b = N_b/\pi r_b^2 a_{22}a_{33}$. From Eqs. (9), (12), (13), (15), and (16), we obtain a system of ordinary differential equations for the matrix $a_{ij}$ components:

$$\ddot{a}_{22} = -\frac{4\pi e^2}{m_e\gamma_e}\left[\frac{A_{33}n_0a_{22}}{A_{22}+A_{33}} - \frac{N_b}{\pi r_b^2\gamma_e^2(a_{22}+a_{33})}\right], \qquad (18)$$

$$\ddot{a}_{33} = -\frac{4\pi e^2}{m_e\gamma_e}\left[\frac{A_{22}n_0a_{33}}{A_{22}+A_{33}} - \frac{N_b}{\pi r_b^2\gamma_e^2(a_{22}+a_{33})}\right]. \qquad (19)$$

We see a similarity between these equations and the equations for the charged particle beam dynamics in high-energy accelerators, which are obtained within the framework of the Kapchinskij–Vladimirskij approximation [46] (e.g., see Refs. [47, 48]).

Using the notation

$$a = r_b a_{22}, \quad b = r_b a_{33}, \quad K_2 = \frac{4\pi n_0 e^2 A_{33}}{m_e c^2\gamma_e(A_{22} + A_{33})},$$

and

$$K_3 = \frac{4\pi n_0 e^2 A_{22}}{m_e c^2\gamma_e(A_{22} + A_{33})}$$

and incorporating the transverse emittance effects, we rewrite Eqs. (18) and (19) as

$$a'' + K_2 a = \frac{\varepsilon_2^2}{a^3} + \frac{\xi}{a+b}\,, \qquad (20)$$

$$b'' + K_3 b = \frac{\varepsilon_3^2}{b^3} + \frac{\xi}{a+b}\,, \qquad (21)$$

where $\varepsilon_2$ and $\varepsilon_3$ are the transverse emittance values in the $y$ and $z$ directions, $\xi = N_b/\pi n_0 r_b^2\gamma_e^2$ is a dimensionless space-charge parameter, and the primes denote differentiation with respect to the variable $s = ct$. Properties of this system of equations are discussed in detail in Ref. [47].

Equations (20) and (21) can be presented in the Hamiltonian form with the Hamiltonian depending on the canonical coordinates $a$ and $b$ and on the canonical momenta $\pi_2$ and $\pi_3$. It is given by

$$\mathcal{H}(\pi_2, \pi_3, a, b) = \frac{1}{2}\left(\pi_2^2 + \pi_3^2 + K_2a^2 + \right.$$
$$\left. + K_3b^2 + \frac{\varepsilon_2^2}{a^2} + \frac{\varepsilon_3^2}{b^2}\right) - \xi\ln(a+b), \qquad (22)$$

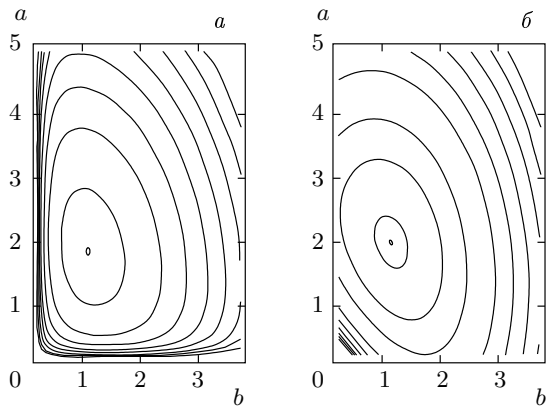


**Fig. 7.** Isocontours of the potential function $\Pi(a,b)$ for *a*) $K_2 = 2.5$, $K_3 = 5$, $\varepsilon_2 = 1$, $\varepsilon_3 = 1$, and $\xi = 1$ and *b*) for $K_2 = 1$, $K_3 = 2.25$, $\varepsilon_2 = 1$, $\varepsilon_3 = 1$, and $\xi = 5$

from which we conclude that for $a > 0$ and $b > 0$, the bunch performs nonlinear oscillations around the equilibrium. In Fig. 7, we plot isocontours of the potential function,

$$\Pi(a,b) = \frac{1}{2}\left(K_2 a^2 + K_3 b^2 + \frac{\varepsilon_2^2}{a^2} + \frac{\varepsilon_3^2}{b^2}\right) - \\ - \xi \ln(a+b), \quad (23)$$

for $K_2 = 2.5$, $K_3 = 5$, $\varepsilon_2 = 1$, $\varepsilon_3 = 1$, and $\xi = 1$ in frame (*a*), and for $K_2 = 1$, $K_3 = 2.25$, $\varepsilon_2 = 1$, $\varepsilon_3 = 1$, and $\xi = 5$ in frame (*b*). From the form of the potential function $\Pi(a,b)$, we can see that in the general case, the frequencies of the oscillations along the $y$ and $z$ directions are different and depend on the oscillation amplitudes. If the emittances $\varepsilon_2$ and $\varepsilon_3$, which are determined by the injection mechanism, vanish, as in Fig. 7*b*, the isocontours of $\Pi(a,b)$ can intersect the axis at $a = 0$ or $b = 0$. This corresponds to the case where one semi-axis of the bunch becomes equal to zero in nonlinear oscillations and the bunch aspect ratio formally tends to infinity. We note that in the axially symmetric configuration, the space-charge effect prevents the bunch radius from vanishing. For a flat electron beam, the space-charge effects are not strong enough and the bunch demagnification in one of the directions becomes possible.

The transverse equilibrium of the electron bunch in the wake corresponds to the local minimum of the function $\Pi(a,b)$ given by Eq. (23). It is obtained by a static solution of Eqs. (20) and (21) for which the terms in the right-hand sides vanish. We consider the case where the emittances vanish. Solving these algebraic equations with $\varepsilon_2 = 0$ and $\varepsilon_3 = 0$, we obtain

$$a^{eq} = \sqrt{\xi \frac{K_2}{K_3}}, \quad b^{eq} = \sqrt{\xi \frac{K_3}{K_2}} \quad (24)$$

for the equilibrium. We point out that in equilibrium, the electron bunch has an elliptic cross section with the aspect ratio $a^{eq}/b^{eq}$ equal to the aspect ratio of the wake: $a^{eq}/b^{eq} = A_{22}/A_{33}$. The electron density inside the bunch in the equilibrium is equal to

$$n_b^{eq} = \frac{N_b}{\pi r_b^2 ab} = n_0 \gamma_e^2. \quad (25)$$

It is $\gamma_e^2$ times greater than the ion density in the plasma. The characteristic transverse size $r_b$ of the bunch can be found as

$$r_b = \sqrt{\frac{N_b}{\pi n_0 \gamma_e^2}}, \quad (26)$$

i.e., the dimensionless space charge parameter $\xi = N_b/\pi n_0 r_b^2 \gamma_e^2$ is equal to unity, $\xi = 1$, for the equilibrium configuration.

Using definition (26) of the transverse size $r_b$ of the bunch and linearizing Eqs. (20) and (21) in the vicinity of the equilibrium solution (24) with $\varepsilon_2 = 0$, $\varepsilon_3 = 0$, $a^{eq} = \sqrt{A_{22}/A_{33}}$, and $b^{eq} = \sqrt{A_{33}/A_{22}}$, i.e., representing the functions $a$ and $b$ as $a = a^{eq} + \delta a$ and $b = b^{eq} + \delta b$ with $\delta a \ll a$ and $\delta b \ll b$, we obtain

$$\delta\ddot{a} = -\omega_b^2 \left\{ \left[ \frac{A_{33}}{A_{22}+A_{33}} + \frac{A_{22}A_{33}}{(A_{22}+A_{33})^2} \right] \delta a + \right. \\ \left. + \frac{A_{22}A_{33}}{(A_{22}+A_{33})^2} \delta b \right\}, \quad (27)$$

$$\delta\ddot{b} = -\omega_b^2 \left\{ \frac{A_{22}A_{33}}{(A_{22}+A_{33})^2} \delta a + \right. \\ \left. + \left[ \frac{A_{22}}{A_{22}+A_{33}} + \frac{A_{22}A_{33}}{(A_{22}+A_{33})^2} \right] \delta b \right\}. \quad (28)$$

These equations describe oscillations with the frequencies

$$\omega_1^b = \omega_b, \quad \omega_2^b = \omega_b \sqrt{\frac{2A_{22}A_{33}}{A_{22}+A_{33}}}. \quad (29)$$

As we see, for $A_{22} \ll A_{33}$, the frequency $\omega_2^b$ is much lower than $\omega_1^b$. We also see that the frequency values in the case where the space-charge effect is taken into account, Eq. (29), are different from the frequencies in Eq. (10) obtained within the framework of the test-particle approximation.

The structure of the mode is described by the relations

$$\begin{pmatrix} \delta a \\ \delta b \end{pmatrix} = \frac{1}{A_{22}^2 + A_{33}^2} \times$$

$$\times \begin{pmatrix} A_{33} & A_{22} \\ -A_{22} & A_{33} \end{pmatrix} \begin{pmatrix} \sum\limits_{\pm} C_{1,\pm} \exp(\pm i\omega_1^b t) \\ \sum\limits_{\pm} C_{2,\pm} \exp(\pm i\omega_2^b t) \end{pmatrix}, \quad (30)$$

where $C_{1,\pm}$ and $C_{2,\pm}$ are constants given by the initial conditions. This expression corresponds to the skewed ellipse form of the potential energy isocontours in the vicinity of the bunch equilibrium position presented in Fig. 7*b*.

## 6. DISCUSSION AND CONCLUSION

In conclusion, a method is suggested for electron injection via transverse wake wave breaking, when the electron trajectory self-intersection leads to the formation of an electron bunch elongated in the transverse direction. In this scheme, we use a laser pulse focused into an elongated spot. This results in a wakefield generation localized in the axially nonsymmetric region with the components of the transverse electric field not equal to each other. With the aid of catastrophe theory, we demonstrate that a structurally stable regime of transverse wake breaking leads to the transversally elongated electron bunch generation. Three-dimensional particle-in-cell simulations of the laser pulse interaction with an underdense plasma show that electrons injected via the transverse wake wave breaking form a bunch with an aspect ratio larger than unity, which qualitatively confirms the theory. Electrons accelerated by the wake perform betatron oscillations with different amplitudes and frequencies along two transverse coordinates. An exact analytic solution of the electron hydrodynamics equations demonstrates the space-charge effects, which modify the electron bunch equilibrium and the frequencies and structure of the mode of betatron oscillations.

For a typical total number of electrons in the bunch accelerated by the wake equal to $N_{tot} = 10^{10}$, which corresponds to the charge 1.6 nC, and the bunch length 10 $\mu$m, the electron number per unit length is $N_b = 10^{13}$ cm$^{-1}$. If the plasma density and electron gamma factor are $n_0 = 10^{19}$ cm$^{-3}$ and $\gamma_e = 500$, expression (26) yields the bunch size in the transverse direction as $r_b \approx 0.01$ $\mu$m. In this case, betatron frequencies (29) are $\omega_1^b \approx 10^{14}$ s$^{-1}$ and $\omega_2^b \approx 1.4 \cdot 10^{13}$ s$^{-1}$, if we assume that the aspect ratio $A_{22}/A_{33}$ equals 100.

One of the most important applications of laser-produced relativistic electrons is to generate positron bunches for their injection into conventional accelerators. To obtain polarized positron beams, an additional circularly polarized laser pulse (counterpropagating with the electron bunch) may be used to generate longitudinally polarized gamma-ray photons, which then collide with a thin-film target [49].

The emittance of laser-accelerated ions can also be manipulated by changing the structure of either the target irradiated by the laser pulse or the form of the focusing system. In the first case, we refer to the double-layer target proposed in Ref. [50] in order to produce beams with controlled quality, and studied in detail via computer simulations [51] and experiments [52]. The authors of Ref. [50] proposed using two-layer targets in which the first layer consists of heavy multicharged ions and the second layer (thin and narrow in the transverse direction) consists of light ions (e.g., protons). Elongating the thin proton layer in one direction results in the generation of a flat proton beam. A more complex form of the proton layer may be used to provide a uniform irradiation of the target, which is required in the applications of laser-accelerated ions for hadron therapy. The second case uses an ion focusing technique corresponding to a thin hollow cylindrical shell irradiated by a femtosecond high-power laser pulse when the ion bunch flies through it. As demonstrated in the experiments in Ref. [53], this technique allows simultaneously focusing the proton beam and cuting it into quasi-monoenergetic beamlets. The use of an elliptical cylinder shell provides a way for transverse emittance manipulation. In addition, a phase rotator, which also produces quasi-monoenergetic ion beamlets [54] when its transverse electric field is made anisotropic, can produce flat ion beams.

This work is supported by the Japanese Ministry of Education, Science, Sports and Culture, Grant-in-Aid for Specially Promoted Research No. 15002013. One of the authors (M. K.) is supported by the Japanese Ministry of Education, Science, Sports and Culture, Grant-in-Aid for Young Scientists (B), No. 17740272, 2005.

## REFERENCES

1. T. Tajima and J. M. Dawson, Phys. Rev. Lett. **43**, 267 (1979).

2. L. M. Gorbunov and V. I. Kirsanov, Zh. Eksp. Teor. Fiz. **93**, 509 (1987).

3. S. V. Bulanov, V. I. Kirsanov, and A. S. Sakharov, Pis'ma Zh. Eksp. Teor. Fiz. **50**, 198 (1989).

4. N. E. Andreev, L. M. Gorbunov, V. I. Kirsanov et al., Pis'ma Zh. Eksp. Teor. Fiz. **55**, 550 (1992).

5. E. Esarey, P. Sprangle, J. Krall, and A. Ting, IEEE Trans. Plasma Sci. **24**, 249 (1996); V. Malka, S. Fritzler, E. Lefebvre et al., Science **298**, 1596 (2002); G. Mourou, T. Tajima, and S. V. Bulanov, Rev. Mod. Phys. **78**, 309 (2006).

6. D. Umstadter, J.-K. Kim, and E. Dodd, Phys. Rev. Lett. **76**, 2073 (1996); E. Esarey, R. F. Hubbard, W. Leemans, A. Ting, and P. Sprangle, Phys. Rev. Lett. 79, 2682 (1997); H. Kotaki, S. Masuda, M. Kando, J. Koga, and K. Nakajima, Phys. Plasmas **6**, 3296 (2004).

7. K. Nakajima, D. Fisher, T. Kawakubo et al., Phys. Rev. Lett. **74**, 4428 (1995); A. Modena, Z. Najmudin, A. E. Dangor et al., Nature (London) **377**, 606 (1995).

8. S. P. D. Mangles, C. D. Murphy, Z. Najmudin et al., Nature (London) **431**, 535 (2004).

9. C. G. R. Geddes, Cs. Toth, J. van Tilborg et al., Nature (London) **431**, 538 (2004).

10. J. Faure, Y. Glinec, A. Pukhov et al., Nature (London) **431**, 541 (2004).

11. K. Koyama, E. Miura, S. Kato et al., J. Particle Accel. Soc. Jpn. **1**, 158 (2004).

12. W. P. Leemans, B. Nagler, A. J. Gonsalves et al., Nature Phys. **2**, 696 (2006).

13. See for example Linac Coherent Light Source Conceptual Design Rep., SLAC-R-593, April 2002, UC-414.

14. Superconducting Electron-Positron Linear Collider Technical Design Rep., DESY Lab. Rep., http://tesla.desy.de/new_pages/TDR_CD/start.html; The Int. Linear Collider Global Design Effort Baseline Configuration Document, http://www.linearcollider.org/wiki/.

15. G. Mortgaat-Pick et al., E-print archives, hep-ph/0106155.

16. K. S. Kumar, R. Roy, P. E. Reimer, and M. Strovink, eConfC010630, SLAC-R-599, eProc. Snowmass 2001; R. Pitthan, http://www-project.slac.stanford.edu/lc/local/Fixed_Target/Pitthan_NLC_Fixed_Target.pdf.

17. R. Pitthan, Snowmass 2001, http://www-project.slac.stanford.edu/lc/local/XFel/FutureEmitNeeds.pdf.

18. T. Raubenheimer and F. Zimmermann, Rev. Mod. Phys. **72**, 95 (2000).

19. A. Chao, R. Pitthan, T. Tajima, and A. Yeremian, Phys. Rev. ST Accel. Beams **6**, 024201 (2003).

20. A. Yamazaki, H. Kotaki, I. Daito et al., Phys. Plasmas **12**, 093101 (2005); T. Hosokai, K. Kinoshita, T. Ohkubo et al., Phys. Rev. E **73**, 036407 (2006); B. Hidding, K.-U. Amthor, B. Liesfeld et al., Phys. Rev. Lett. **96**, 105004 (2006); M. Mori, M. Kando, I. Daito et al., Phys. Lett. A **356**, 146 (2006); C.-T. Hsieh, C.-M. Huang, C.-L. Chang et al., Phys. Rev. Lett. **96**, 095001 (2006).

21. S. V. Bulanov, M. Yamagiwa, T. Zh. Esirkepov et al., Phys. Plasmas **12**, 073103 (2005).

22. T. Esirkepov, S. V. Bulanov, M. Yamagiwa, and T. Tajima, Phys. Rev. Lett. **96**, 014803 (2006).

23. D. Edwards et al., 2001 Particle Accelerator Conf., http://accelconf.web.cern.ch/AccelConf/p05/papers/WPAP035.pdf.

24. J. Faure, C. Rechatin, A. Norlin, A. Lifschitz, Y. Glinec, and V. Malka, Nature (London) **444**, 737 (2006).

25. J. M. Dawson, Phys. Rev. **133**, 383 (1959).

26. A. I. Akhiezer, I. A. Akhiezer, R. V. Polovin, A. G. Sitenko, and K. N. Stepanov, *Plasma Electrodynamics*, Pergamon, Oxford (1975).

27. S. V. Bulanov, F. Pegoraro, A. M. Pukhov, and A. S. Sakharov, Phys. Rev. Lett. **78**, 4205 (1997).

28. T. V. Liseikina, F. Califano, V. A. Vshivkov et al., Phys. Rev. E **60**, 5991 (1999); A. Pukhov and J. Meyer-ter-Vehn, Appl. Phys. B **74**, 355 (2002); H. Xu, W. Yu, P. Lu et al., Phys. Plasmas **12**, 013105 (2005).

29. S. V. Bulanov, V. I. Kirsanov, and A. S. Sakharov, Pis'ma Zh. Eksp. Teor. Fiz. **53**, 540 (1991); C. A. Coverdale et al., Phys. Rev. Lett. **74**, 4659 (1995); D. Gordon et al., Phys. Rev. Lett. **80**, 2133 (1998).

30. A. Zhidkov et al., Phys. Rev. E **69**, 035401(R) (2004).

31. S. V. Bulanov, N. M. Naumova, F. Pegoraro, and J. Sakai, Phys. Rev. E **58**, R5257 (1998); H. Suk, N. Barov, J. B. Rosenzweig, and E. Esarey, Phys. Rev. Lett. **86**, 1011 (2001).

32. N. Hasegawa et al., JAERI Review 2001-003, p. 31 (2001); I. N. Ross et al., Appl. Opt. **26**, 1854 (1987).

33. S. V. Bulanov and A. S. Sakharov, Pis'ma Zh. Eksp. Teor. Fiz. **54**, 208 (1991).

34. N. H. Matlis et al., Nature Phys. **2**, 749 (2006).

**35**. T. Poston and Y. Steward, *Catastrophe Theory and its Applications*, Pitman, London (1978).

**36**. S. V. Bulanov, T. Zh. Esirkepov, and T. Tajima, Phys. Rev. Lett. **91**, 085001 (2003).

**37**. C. D. Murphy et al., Phys. Plasmas **13**, 033108 (2006).

**38**. T. Zh. Esirkepov, Comput. Phys. Comm. **135**, 144 (2001).

**39**. A. Macchi et al., in: *Proc. of 42nd Annual Meeting of the APS Division of Plasma Physics and 10th Int. Congress on Plasma Physics*, Québec City (2000), Book of Abstracts, Paper MP1.065.

**40**. S. P. D. Mangles, A. G. R. Thomas, M. C. Kaluza et al., Phys. Rev. Lett. **96**, 215001 (2006).

**41**. S. Chandrasekhar, *Ellipsoidal Figures of Equilibrium*, Yale Univ., New Haven (1969); L. D. Landau and E. M. Lifshitz, *Electrodynamics of Continuous Media*, Pergamon, New York (1960).

**42**. L. I. Sedov, *Similarity and Dimensional Methods in Mechanics*, Academic, New York (1959).

**43**. G. K. Batchelor, *An Introduction to Fluid Mechanics*, Cambridge Univ. Press, Cambridge (1967).

**44**. Ya. B. Zel'dovich, Astron. Astrophys. **5**, 84 (1970); Ya. B. Zel'dovich and I. D. Novikov, *The Structure and Evolution of the Universe*, Univ. Chicago Press, Chicago and London (1983).

**45**. V. S. Imshennik and S. I. Syrovatskii, Sov. Phys. JETP **52**, 900 (1967); S. V. Bulanov and M. A. Ol'shanetskij, Sov. J. Plasma Phys. **11**, 425 (1985); T. Tajima and J.-I. Sakai, Sov. J. Plasma Phys. **15**, 606 (1989); S. V. Bulanov and J.-I. Sakai, Astrophys. J. Suppl. Ser. **117**, 599 (1998).

**46**. I. M. Kapchinskij and V. V. Vladimirskij, in *Proc. 2nd Int. Conf. on High Energy Accelerators and Instruments*, CERN, Geneva (1959), p. 274.

**47**. A. W. Chao, *Physics of Collective Beam Instabilities in High Energy Accelerators*, John Wiley and Sons, New York (1993).

**48**. S. Humphries, Jr., *Charged Particle Beams*, John Wiley and Sons, New York (1990).

**49**. T. Omori, M. Fukuda, T. Hirose et al., Phys. Rev. Lett. **96**, 114801 (2006).

**50**. S. V. Bulanov and V. S. Khoroshkov, Plasma Phys. Rep. **28**, 453 (2002).

**51**. S. V. Bulanov, T. Zh. Esirkerov, V. S. Khoroshkov et al., Phys. Lett. A **299**, 240 (2002); T. Zh. Esirkerov, S. V. Bulanov, K. Nishihara et al., Phys. Rev. Lett. **89**, 175003 (2002); E. Fourkal, I. Velchev, J. Fan, W. Luo, and C.-M. Ma, Med. Phys. **34**, 577 (2007).

**52**. C. Schwoerer et al., Nature **439**, 445 (2006).

**53**. T. Toncian, M. Borghesi, J. Fuchs et al., Science **312**, 410 (2006); M. Dunne, Science **312**, 374 (2006).

**54**. A. Noda, S. Nakamura, Y. Iwashita et al., Laser Phys. **16**, 647 (2006).